

Post Access Report

Experimental Performance Characterization of a Shrouded
Axial-Flow Turbine

Awardee: Sitkana

Awardee point of contact: Lance McMullan

Facility: University of Washington – Harris Hydraulics: Alice C.
Tyler Flume

Facility point of contact: Brian Polagye

Authors: Lance McMullan, Brian Polagye, Gemma Calandra,
Greg Talpey, Katherine Van Ness

Date: 13 February 2024

EXECUTIVE SUMMARY

The objective of this project was to characterize the performance of Sitkana’s shrouded axial-flow turbine rotor. The purpose of the shroud is to provide structural integrity while using thin blades which can reduce the material cost of the rotor. In addition, the shroud minimizes the risk of contact between marine animals and the rotor tips.

This project allowed Sitkana to (1) refine the optimal rotor geometry, (2) validate their numerical models, and (3) predict power output for a full-scale system. First, Sitkana used a computational fluid dynamic program to iteratively improve rotor design. Eleven rotors were selected, manufactured, and sent to the University of Washington to characterize rotor performance. The team at UW tested these rotors experimentally in the Alice C. Tyler Flume and analyzed the coefficients of power and thrust.

The results indicated that two variants (identified as rotor #1 and rotor #2, with rotor #2 having a higher height-to-diameter ratio) performed the best of the shrouded rotors with similar blockage-corrected power coefficients of 0.21 (Fig. 1). Of these, rotor #1 had a lower thrust coefficient value. The power coefficient of 0.21 is sufficient to drive the generators that Sitkana plans to incorporate into a full-scale (1-meter diameter) prototype, indicating the project objective was successfully achieved.

With these results, Sitkana is positioned to build a full-scale prototype with an understanding of potential power output. Both rotors #1 and #2 should be further investigated in an open water setting to further assess performance.

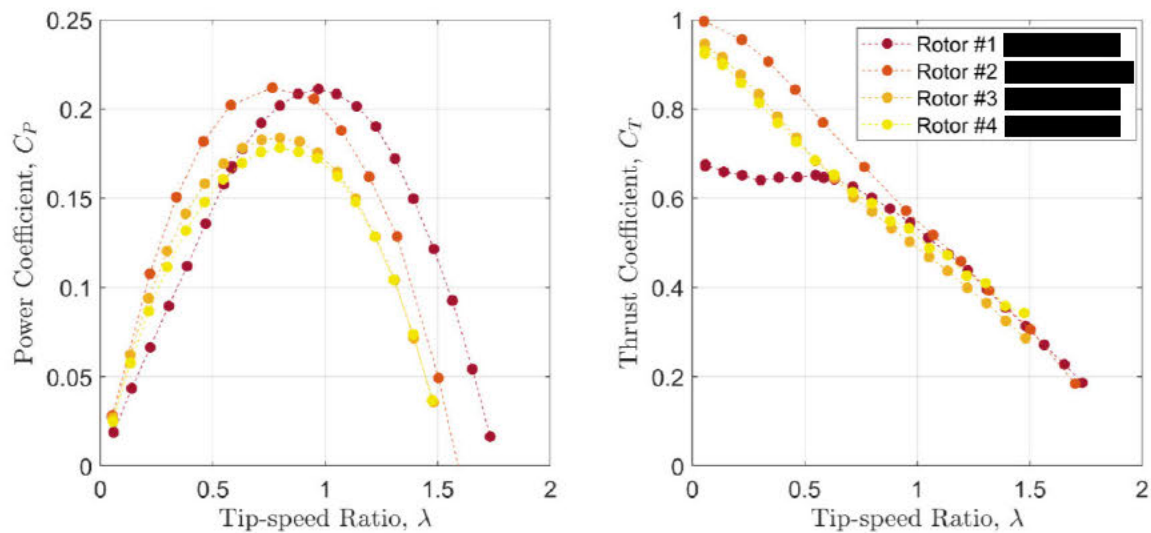


Figure 1. Blockage-corrected coefficients of power and thrust as a function of tip-speed ratio for shrouded rotors of varying height-to-diameter ratios. Shades from dark to light indicate increasing height-to-diameter ratios.

1 INTRODUCTION TO THE PROJECT

Sitkana has developed a shrouded hydrokinetic turbine with a modular, low-cost design that can be scaled to meet the needs of remote communities. With technical support from the University of Washington, Sitkana sought to experimentally characterize the mechanical power and structural loads of various 1:3.3 scale rotor geometries. In all, 11 different rotor geometries were characterized with variations in height-to-diameter ratio, blade number, and blade type (foiled versus flat). All tests were conducted in Reynolds-independent flow conditions in the Alice C. Tyler Flume at the University of Washington. This scale model characterization allows Sitkana to (1) refine the optimal rotor geometry, (2) validate their numerical models, and (3) predict power output for a full-scale system.

2 ROLES AND RESPONSIBILITIES OF PROJECT PARTICIPANTS

2.1 APPLICANT RESPONSIBILITIES AND TASKS PERFORMED

Sitkana (the applicant) designed and printed 11 turbine rotor geometries to be tested. Following testing, the Sitkana team reviewed the performance data and co-authored the post-access report.

2.2 NETWORK FACILITY RESPONSIBILITIES AND TASKS PERFORMED

University of Washington (UW, the facility) performed experiments to characterize the turbine rotors provided by Sitkana. UW designed and 3D-printed a cap that mounts onto the existing test rig hub to provide an attachment point for testing the rotors provided by Sitkana. The testing process will include:

- Set-up and verification that all data streams are functioning on the axial-flow test rig;
- Determining flow conditions under which the test articles achieve Reynolds-independence;
- Full performance characterization of the test articles at Reynolds-independent conditions; and
- Data post-processing, including non-dimensionalization and blockage correction.

Additionally, UW was responsible for compiling the results of the experiments and leading the development of the post-access report.

3 PROJECT OBJECTIVES

The purpose of this test was to experimentally characterize scale-model turbine performance for rotors designed to address the high cost of and environmental concerns with existing marine current turbine technology. The high cost of marine energy technology is due, in part, to the expensive, corrosive-resistant composite blades. Sitkana's technology operates on a smaller scale and so is subjected to lower forces, allowing the use of common polymer materials. This is expected to reduce material costs and allow for rapid manufacturing. Additionally, the most powerful tidal currents in North America are in Alaskan waters where there are high-profile wildlife like orcas, seals and humpback whales. Because current turbines pose a collision risk, Sitkana's turbine was designed with an integrated shroud that contains the blade tips. This is expected to substantially reduce the risk posed to marine mammals.

Sitkana developed numerical models of turbine performance to optimize rotor geometry and evaluate the feasibility of additive manufacturing for turbines with a power output on the order of 5 kW. These models require experimental validation. The objective of this work is to experimentally characterize scale-model turbine performance with respect to power generation and structural loads. The results of these tests allow Sitkana to validate their numerical models and proceed to the next phase of development.

4 TEST FACILITY, EQUIPMENT, SOFTWARE, AND TECHNICAL EXPERTISE

The University of Washington's Alice C. Tyler Flume was selected based on the following considerations:

- The Alice C. Tyler Flume can produce constant, uniform flow up to 1.1 m/s with low turbulence intensities (1-4%) and, based on prior results, can reach Reynolds-independent conditions for turbines of scale similar to Sitkana's 1:3.3 scale rotors. An acoustic Doppler velocimeter (Nortek Vector) is available to collect point measurements upstream of the turbine.
- The facility can provide an instrumented axial-flow test rig capable of measuring six-axis loads on the rotor and rotation rate to determine turbine performance and structural loads. The relevant data acquisition and post-processing scripts are also available from prior axial-flow turbine research.
- The equipment, hardware, and software used for this project have been successfully demonstrated and utilized for ongoing research at UW for the past seven years.
- Critical personnel with extensive experience in experimental testing with the axial-flow test rig will be available to assist Sitkana in collecting, processing, and analyzing data outlined in the proposed test plan.
- Sitkana is a Seattle-based company with all co-founders living within thirty minutes of the University of Washington.

5 TEST OR ANALYSIS ARTICLE DESCRIPTION

Sitkana's hydrokinetic generator system will be used to generate renewable energy from flowing water through the rotation of a shrouded axial-flow turbine. Hydrokinetic technology adoption has been slowed by two major obstacles that Sitkana's technology is attempting to solve: (1) the high cost of building equipment that can survive marine environments, and (2) environmental concerns associated with submerging equipment in marine environments. Sitkana's integrated shrouded turbine aims to provide a lower cost and lower impact alternative to the solutions currently available.

Marine equipment is expensive due to the requirements of withstanding both the corrosive salt water and the high forces of water currents. Leading competitors, such as Nova Innovation and Orbital Marine Power, use composite materials for their blades which extend outward from a central point, analogous to standard wind turbine technology.

Due to the smaller size of Sitkana's turbines (1 m radius versus 4.25 m and 10 m for Nova Innovation and Orbital Marine Power), the turbine is subjected to less overall thrust, so the materials require less strength. This should allow Sitkana to use common polymers like ABS, PVC, or PET in turbine construction instead of composites. The use of common polymers and simple geometry should enable rapid manufacturing. Additionally, the turbine blades of Sitkana's design are of uniform thickness. As

seen in Fig. 2, the geometry of the turbine is formed by twisting the flat planes of the turbine about its axis of rotation, keeping the base fixed. This is different from traditional hydrokinetic technologies that utilize hydrofoil principles. Sitkana's turbine does not operate by using lift; instead, the turbine rotates due to the normal force against the blade surface creating a moment about the axis of rotation.



Figure 2. Sitkana's integrated shrouded turbine geometry, illustrating that it can be formed by repetitively stacking the initial shape, twisting and shrinking each layer.

When additively manufactured, each layer comprises straight lines which minimizes wear on the printer and reduces the likelihood of printing failure, saving time and material waste. The straight-line geometry also allows for eventual rotational injection molding to create turbines as single formed pieces.

A common obstacle for hydrokinetic power technologies is permitting due to environmental regulatory concerns about potential wildlife impact. Sitkana's system has been designed to minimize wildlife impact through the use of an integrated turbine shroud and intake protection. The purpose of the integrated turbine shroud is to reduce the collision risk from free blade tips. When the turbine is in operation, the shroud presents a smooth surface from the side angles (Fig. 3). This feature should help prevent potential impact to larger marine life, such as cetaceans or pinnipeds, because if they collide with the device, there will be no rotating edges to slice or impact them. The purpose of the protective fins attached to the device body (Fig. 4) are to deter large objects from entering or striking the turbine. The protective fins act as a filter for the turbine; larger objects should be redirected outside of the shroud, while smaller objects should pass through the fins and turbine unharmed.

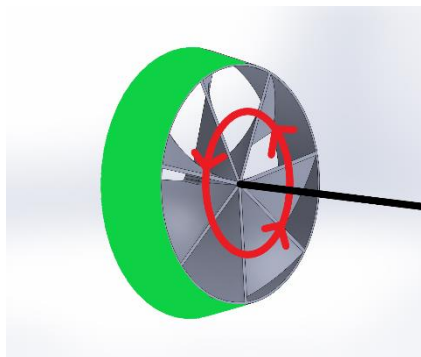


Figure 3. Visual representation of the smooth surface of the shroud (green) while the device is rotating about a central axis (black).

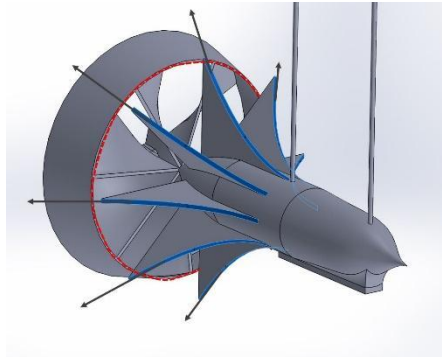


Figure 4. Full hydrokinetic device body, highlighting the protective fins' (blue) purpose of deflecting objects around the device inlet (red).

Each cost saving and wildlife protective measure has a negative impact on the efficiency of the hydrokinetic system. The protective fins decrease the current velocity entering the turbine. The integrated shroud increases thrust and adds parasitic torque. The foil-less blades are likely less efficient than foiled counterparts. Additive manufacturing produces uneven surfaces that will increase drag. Sitkana believes that these could all be worthwhile trade-offs if the technology is able to proceed more quickly through the regulatory approvals, be deployed in large numbers, and be rapidly produced at low cost.

The shrouded turbine geometry can be fully described through five parameters (Fig. 5). In preparation for TEAMER testing, Sitkana identified tentative values for each parameter using a computational fluid dynamic (CFD) simulation program, resulting in 11 turbine rotors, 30 cm in diameter. The CFD modeling helped to identify nonlinear interactions between the design parameters and allowed Sitkana to test multiple local maxima identified by design optimization. The values for each design parameter used in the optimization are as follows:

- (1) shroud draft angle: 0°
- (2) blade twist angle: [REDACTED]
- (3) height-to-diameter ratio: [REDACTED]
- (4) thickness-to-height ratio: 0.04
- (5) blade number: 7-11

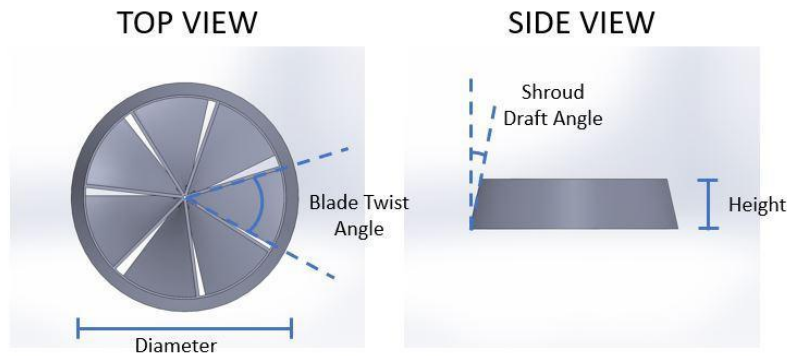


Figure 5. Shrouded turbine geometry with blade twist angle, shroud draft angle, height and diameter are shown. For this example, blade number is seven, and wall thickness will always be the minimum required for material integrity.

In addition to varying the five geometric parameters in the test articles, Sitkana was also interested in analyzing the effect of a foiled (NACA 8212 profile) versus flat blade shrouded turbine. Foiled blades increase material use and cost, as well as increasing manufacturing difficulty. It is important to understand if the expected increase in efficiency outweighs these factors, so two of the test articles used foiled, instead of flat, blades. Finally, the effect of the shroud on turbine performance was also explored by including two test articles without a shroud. A summary of all 11 rotor variants and their defining characteristics is included in Table 1.

Table 1. Summary of each rotor variant. Foiled blades used a NACA 8212 profile.

Rotor #	Blade No.	Shroud Y/N	Blade type	Twist	Height/Diameter
1	9	Y	Flat	■	■
2	9	Y	Flat	■	■
3	9	Y	Flat	■	■
4	9	Y	Flat	■	■
5	9	Y	Foiled	—	-
6	9	N	Foiled	—	-
7	9	N	Flat	■	■
8	8	Y	Flat	■	■
9	7	Y	Flat	■	■
10	10	Y	Flat	■	■
11	11	Y	Flat	■	■

6 WORK PLAN

6.1 EXPERIMENTAL SETUP, DATA ACQUISITION SYSTEM, AND INSTRUMENTATION

Experiments with each rotor design provided by Sitkana were conducted in the Alice C. Tyler Flume, a recirculating open-channel flume with a test section 0.6 meter in depth and 0.76 meter in width. During tests, flow velocity, water temperature, and water free surface height were measured. Flow velocity was measured 3-diameters upstream of the rotor plane using an acoustic Doppler velocimeter (Nortek Vector, 25 Hz sampling rate). Water temperature was monitored by a thermometer in the stilling basin. Free surface height was measured with a free surface transducer (Omega, 1 Hz sampling rate) during the lowest and highest flow speeds to capture the change in dynamic water height.

The Sitkana rotor performance was calculated using angular velocity of the driveshaft motor and measurements from the six-axis load cell (ATI Industrial Automation, Mini45) on board the test rig hub. The test rig hub has been used for over seven years for axial-flow turbine experiments, including multiple peer-reviewed publications (e.g., Van Ness et al. 2021). An optical encoder typically verifies the azimuthal position of the motor but was not operational during the time of testing. However, stepper motors are known for their precise speed control, and prior testing with this axial-flow turbine has demonstrated that we achieve the commanded rotation rate within 0.3% error. The load cell measures torques and forces around/along three perpendicular axes and these voltage signals are digitally transmitted and acquired by a desktop computer at a sampling rate of approximately 25 Hz. Load cell voltages are then transformed into forces and torques using the manufacturer's calibrations for the load cell. The drive train and instrumentation layout is detailed in Fig. 6. and a summary of the sensors and their range/accuracy is provided in Table 2. Collected data will be immediately processed and analyzed to produce power and thrust coefficients as a function of tip-speed ratio (described in Section 6.5.3) and to monitor data streams during data collection to help identify and correct any errors during testing (described in Section 6.5.2). These experimentally determined coefficients of power and thrust at different operating conditions for each rotor design are intended to assist Sitkana in validating their computational models and in assessing the tradeoffs associated with each rotor design.

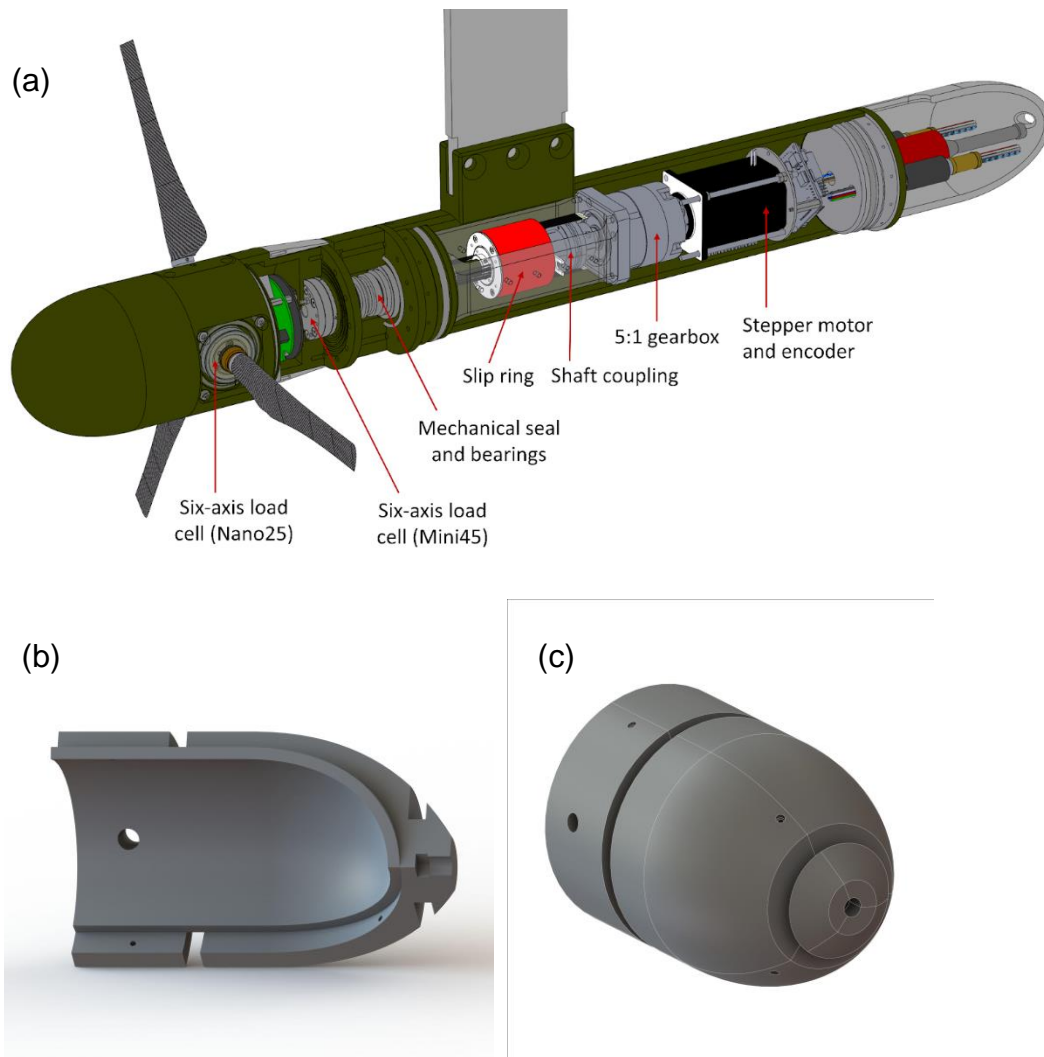


Figure 6. (a) CAD model of turbine and instrumentation. Note that for the test plan, the blades were removed and the rotor designs provided by Sitkana were mounted to the existing hub via (b,c) an interface unit designed and 3D-printed by UW.

Table 2. Summary of sensors used for data acquisition and their range, accuracy, and calibration.

Sensor	Range	Accuracy	Calibration
Force/torque sensor (Mini45, ATI Industrial Automation)	Axial thrust: 270 N Torque: 4.50 Nm	Axial thrust: +/- 2 N Torque: +/- 0.06 Nm	19 Jan. 2023
Acoustic Doppler velocimeter (Nortek Vector)	+/- 0.3, +/- 1.0, +/- 2 m/s (software-selectable)	+/- 0.5% of measured value +/- 1 mm/s	27 Sept. 2013
Free surface transducer (Omega, LVU32)	0.18-2.50 m	+/- 0.25 mm	New 2014

6.2 TEST AND ANALYSIS MATRIX AND SCHEDULE

Each rotor design provided by Sitkana went through three basic tests described in this section: (1) investigation of Reynolds-dependence, (2) data collection at Reynolds-independence, and (3) data validation.

As in Van Ness et al. (2021), the Reynolds-independent threshold for each test article was determined by adjusting the Reynolds number using a combination of flow speed and temperature control until performance was found to be invariant to further increases. At each Reynolds number, the turbine was controlled using speed control (i.e., constant angular velocity) over a range of angular velocity set points that produced positive torque on the rotor (i.e., positive power output). A sweep of 10-20 set points for a given rotor and Reynolds number (i.e., temperature and flow speed combination) is considered a single performance curve. Table 3 roughly outlines the number of performance curves required to find or verify Reynolds independent conditions.

Once Reynolds-independent conditions were identified, two sweeps of 10 angular velocity set points were used to fully characterize performance of each rotor geometry. The second sweep served the purpose of (1) validating the initial result from identifying Reynolds independence and (2) increasing data resolution.

As shown in the experimental schedule in Table 4, the first week of experimental testing was used for setup, fine tuning experimental procedures with the new rotor design, troubleshooting the interface piece, and determining the appropriate range and resolution of angular velocity set points.

Table 3. Experimental test plan.

Test	Reynolds numbers	Rotor Variants	Performance curves	Angular velocity set points per curve	Estimated Experimental Time to Complete
Reynolds Independence	2-4	11	24	10	1 week
Performance	1	11	11	10	0.5 weeks
Validation	1	11	11	10	0.5 weeks

Table 4. Experimental schedule.

Week 1	Experimental setup; fine tuning experimental procedures with the new rotor type; troubleshooting the interface piece, establishing the appropriate range and resolution of angular velocity set points
Week 2	Testing rotor designs 1-6, including Reynolds-dependence investigation and validation
Week 3	Testing rotor designs 7-11, including Reynolds-dependence investigation and validation

6.3 SAFETY

The facility undergoes an annual inspection by the Environmental Health & Safety Department, a University of Washington administrative unit that ensures research laboratories provide a safe place for working. All personnel involved in the proposed project are up to date on all required safety trainings and standard operating procedures on file for the equipment and materials that will be used during the project. The facility has a single track ceiling hoist that is used to move the turbine in and out of the Alice C. Tyler Flume. All personnel that operated the hoist during the project have Overhead and Gantry Crane training and Rigging Safety training and have reviewed the standard operating procedure for this use. When the flume and turbine were operating, all present used hearing protection and safety glasses.

6.4 CONTINGENCY PLANS

A Reynolds-independent regime describes the flow conditions for which turbine performance and normalized thrust on the rotor are invariant to changes in Reynolds number. Conducting lab-scale testing at Reynolds-independence is ideal for scaling to field-scale performance but is not always possible at small facilities. If Reynolds-independence could not be achieved, we planned to use the flow and temperature conditions that produce the highest Reynolds number possible. This would minimize the differences between lab- and full-scale performance while still revealing the relative differences in performance and structural loading between rotor designs.

The 3D printed interface between the existing hub and Sitkana rotors was bench tested prior to testing in the Alice C. Tyler Flume. However, if flume testing revealed that additional alterations to the interface piece were required, we were prepared to make alterations on site and resume testing as soon as possible. Alternatively, if the required alterations could not be performed in a timely manner, we were prepared to delay the remainder of the test schedule until the alterations could be made. Either option might have reduced the number of tests that could be performed, in which case we would have followed the contingency plan outlined below.

If unexpected issues arose and not all tests could be performed, we would have reduced the number of rotor designs to be tested. Sitkana would then have indicated the priority of each rotor design and we would have conducted all the tests for each rotor before moving on to another design to ensure that we obtained all relevant data for the prioritized rotor designs.

6.5 DATA MANAGEMENT, PROCESSING, AND ANALYSIS

6.5.1 Data Management

Raw and processed data is publicly released to the Marine and Hydrokinetic Data Repository (MHK-DR). During and after experimental testing, raw and processed data was stored locally on the data acquisition computer and externally on Dropbox and a data storage server.

The raw data is organized into folders for each performance curve, where each folder contains MATLAB data files containing a time series of force/torque, velocity, free surface height (when available), and rotor speed. The number of set points used in the performance curve during testing will correspond to the number of MATLAB data files included in each folder. The processing code and processed data are also included in the MHK-DR submission. The processed data includes data files (.mat and .csv) for each performance curve with fields for the time-averaged velocity, thrust, power, power coefficient, thrust coefficient, and interquartile range at each tip-speed ratio.

Table 5. Data submitted to the MHK-DR and the data format.

Data to be submitted to the MHK DR	Format
Experimental metadata (test conditions, notes)	Text file
Raw data (time series of force/torque, velocity, rotor speed)	MATLAB data file
Data processing/analysis script	MATLAB script file
Processed data (time-averaged velocity, power/thrust coefficients, interquartile range at each tip-speed ratio for both flume and blockage-corrected conditions)	CSV and MATLAB data file

6.5.2 Data Processing

Collected data was immediately processed and analyzed to produce power and thrust coefficients as a function of tip-speed ratio (described in Section 6.5.3) and to monitor data streams during data collection to help identify and correct any errors during testing.

The following methods were used to detect and prevent erroneous data:

- Time series of the raw load measurements from the force/torque sensor were automatically plotted after data collection at each tip-speed ratio to identify any inconsistencies or measurements outside of the calibration range of the sensor.
- Tare measurements were collected at the start of each performance curve. This provides a consistent baseline for diagnosing unexpected errors in the data and provides a more accurate measurement of force/torque.
- The same set point within a performance curve was repeated at the beginning and end of each test to confirm repeatability and/or adjust for small measurement drift in the force/torque sensor
- The same set points and flow conditions with the first tested rotor (#2) were repeated after Week 1 and Week 2 (Table 4) to confirm repeatability across testing days.
- After a range of set points was tested, the data was immediately processed and analyzed with custom scripts to visualize the power and thrust coefficients as a function of tip-speed ratio. This allowed us to look for inconsistencies, outliers, large shifts in data, exceptional noise, general trends, etc.
- A second sweep of set points at the same flow conditions used to produce the Reynolds-independent performance curves were repeated for each rotor design to validate the primary results of interest in this study.

Measurement uncertainty was quantified and visualized using the interquartile range of the data, which describes its statistical spread around the median values. The interquartile range is calculated by dividing the data into quartiles. The middle quartiles, between the 25th and 75th percentiles of the data were plotted over the mean values to describe their experimental uncertainty.

6.5.3 Data Analysis

For each test article, mechanical power of the turbine was calculated for each rotation rate set point using the reaction torque about the axis parallel to the flow multiplied by the angular velocity of the rotor. This quantity was averaged over 3000 samples (~2 min) at each set point. Similarly, thrust was calculated directly from the force measured by the load cell axis parallel to the inflow. These two quantities were normalized using the energy and momentum flux, respectively, of the freestream inflow passing through the turbine rotor to give coefficients of performance (C_p) and thrust (C_T) as

$$C_p = \frac{\langle \tau \omega \rangle}{\frac{1}{2} \rho A \langle U^3 \rangle} \quad (1)$$

$$C_T = \frac{\langle T \rangle}{\frac{1}{2} \rho A \langle U^2 \rangle} \quad (2)$$

where τ is the mechanical torque, ω is the rotor angular velocity, ρ is the density of water, A is the shroud inlet area, U is the freestream fluid velocity, and T is the thrust acting on the rotor. The rotation rate was normalized by the free stream velocity to give the tip-speed ratio (λ):

$$\lambda = \frac{\omega R}{\langle U \rangle} \quad (3)$$

where R is the shroud's outer radius.

Because the rotor cross-sectional area was an appreciable fraction of the channel cross-sectional area (15.5%), power and thrust were increased by blockage. We corrected the non-dimensional performance characteristics using the method of Barnsley and Wellicome (1990), which has been previously demonstrated (Ross and Polagye 2020) to accurately recover unconfined performance. These values can be used to estimate power production at an increased scale, as well as validate power and force estimates from numerical models.

7 PROJECT OUTCOMES

7.1 RESULTS & DISCUSSION

7.1.1 Reynolds-independence

Hydrodynamic performance can be significantly impacted by Reynolds number, the ratio of inertial to viscous forces. We define the diameter-based Reynolds number as

$$Re_D = UD/\nu, \quad (4)$$

where U is the freestream velocity, D is the turbine diameter, and ν is the kinematic viscosity of the water. Ideally, this parameter would be kept constant between a prototype and full-scale device, but such high Reynolds numbers often cannot be achieved in laboratory-scale facilities. There is, however, a threshold at which nondimensional turbine performance becomes independent of Reynolds number. In this set of experiments, we confirmed Reynolds-independent flow conditions by testing rotor #2 at four different Reynolds numbers in the range $1.2 \times 10^5 - 2.9 \times 10^5$ (Fig. 7). The change in Reynolds number corresponded to changes in flow speed (0.42, 0.55, 0.66, 0.77 m/s) and temperature (20°C, 30°C). We observed no differences in the power or thrust coefficients across this range of Reynolds numbers (Fig. 7). For the remaining rotors, we tested at both $Re_D = 2.1 \times 10^5$ ($T = 30^\circ\text{C}$, $U = 0.55\text{m/s}$) and $Re_D = 2.9 \times 10^5$ ($T = 30^\circ\text{C}$, $U = 0.77\text{ m/s}$) to confirm that we were still Reynolds-independent when operating with the alternate rotor designs. Performance results of rotors #1 and #3-11 at both Reynolds numbers are included in Appendix A, which demonstrate, at most, a few percent change in coefficients of power and thrust for any given turbine. With Reynolds-independence demonstrated for each rotor, the blockage-corrected power and thrust coefficients reported in the following sections can be understood to be representative of a full-scale device.

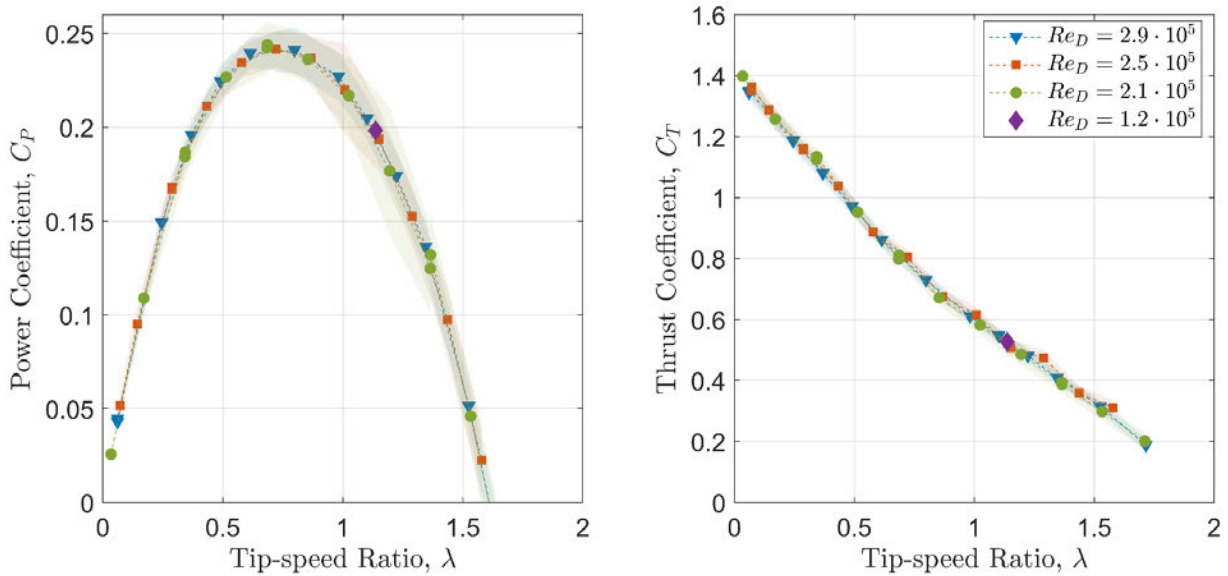


Figure 7. Coefficients of power and thrust as a function of tip-speed ratio for rotor #2 under various Reynolds numbers. Shaded regions indicate the interquartile range.

7.1.2 Hydrodynamic performance

Four investigations are made across the 11 rotor designs tested in the flume: (1) effect of rotor height (along-channel dimension), (2) effect of shroud, (3) effect of foiled versus flat blades, and (4) effect of blade number. Comparisons of turbine performance for each of these design variations are provided to support Sitkana in (1) validating their CFD models and (2) identifying the optimal rotor design based on the expected power and loads and the material cost associated with each design.

Fig. 8 compares four rotor geometries of varying height-to-diameter ratio, [REDACTED]. Optimal tip-speed ratios for each rotor fall between 0.7-1.0. This relatively low tip-speed ratio operating range is typical of high-solidity axial-flow rotors (Borg et al. 2020). We observe the thrust coefficients decrease with an increase in tip-speed ratio, which is also typical of high-solidity rotors (Borg et al. 2020) due to high axial induction (i.e., the fractional decrease between the freestream velocity and the velocity at the rotor plane). When stationary or at low tip-speed ratios, a high-solidity rotor impedes flow through the rotor, increasing static pressure upstream of the rotor and, consequently, increasing the thrust load. This effect is exacerbated by the shroud, which hinders the obstructed flow from passing around the rotor plane. At higher tip-speed ratios, flow rate through the rotor plane increases, resulting in a decrease in C_T .

Maximum C_P and C_T is observed for rotor #2 at 0.242 and 1.36, respectively. Rotor #1 demonstrates a slightly lower C_P at 0.232 but with significant reduction in maximum C_T , which peaks at 0.74. Rotors #3 and #4, with the highest height-to-diameter ratios, perform similarly in C_P and C_T , with a peak CP less than rotors #1 and #2. Note that, due to the rotor design, increasing the height-to-diameter ratio increases rotor solidity, defined as

$$\sigma = A_b/A_r \quad (5)$$

where A_b is the projected frontal area of the blades at rest and A_r is the rotor swept area. This is consistent with the significant difference in peak C_T between rotors #1 and #2, with $\sigma = 0.5$ and $\sigma = 0.875$, respectively, as low rotor solidity allows more flow to pass through the rotor without making contact with the blades. With rotors #3 and #4, where $\sigma = 1.0$ (i.e., project area equal to swept area), we observe a decrease in peak C_T from rotor #2. While there is a small increase in solidity from rotor #2, this appears to be dominated by the inefficiency of the large height-to-diameter ratio, which results in overlapping blades. This arrangement is non-optimal and decreases overall energy capture and corresponding thrust force. The similarity in performance between rotors #3 and #4 suggests that once overlap occurs, further increases in the height-to-diameter ratio have little effect on performance.

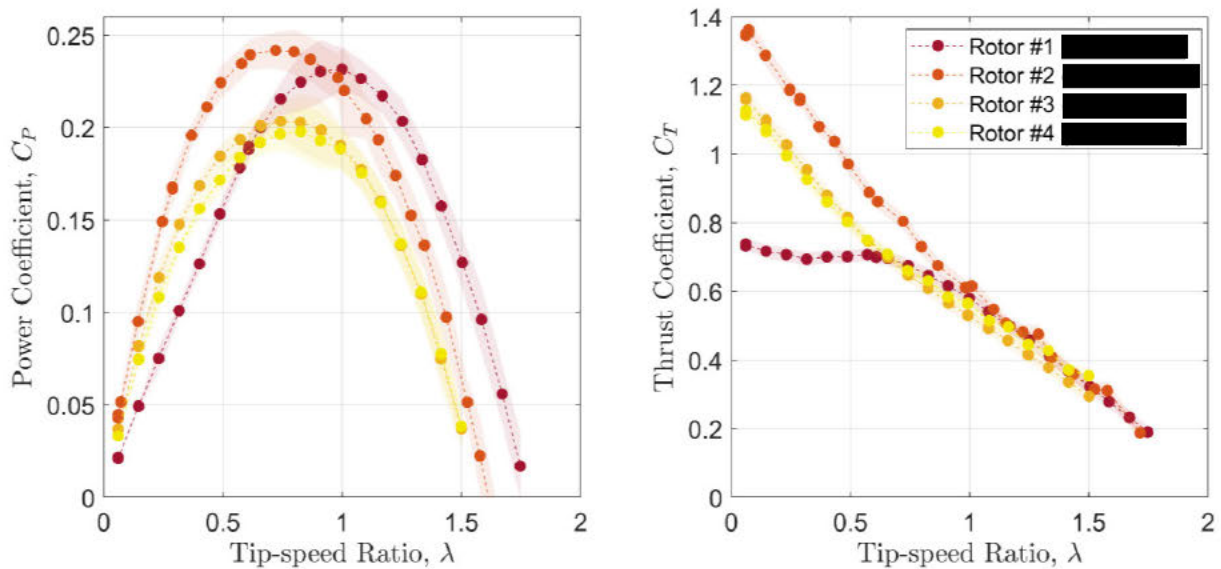


Figure 8. Coefficients of power and thrust as a function of tip-speed ratio for shrouded rotors of varying height-to-diameter ratios. Shaded regions indicate the interquartile range. Shades from dark to light indicate increasing height-to-diameter ratios.

Fig. 9 compares four rotor geometries with flat and foiled blades, both with and without a shroud. The foiled blade geometry is a NACA 8212 profile, with constant chord length and thickness along the entire blade span, varying only in twist from root to tip. For the flat bladed rotor, the shroud resulted in a 7% loss in power and an approximate 0.1 increase in C_T at any given tip-speed ratio. The loss in power can be attributed to drag on the shroud causing a parasitic torque opposing the direction of rotation while the increase in C_T can be attributed to drag on the shroud in the streamwise direction. While the hydrodynamic performance is best without the shroud, it is important to note that we observed, by eye, the blades without the attached shroud deflecting by roughly 1 cm during testing. At the current thickness, the blades may not be able to survive extended field operations without the shroud, unless a

stiffer material is used. With the presented performance results, Sitkana can determine cost/benefit of the material cost required to fabricate a structurally suitable rotor without a shroud compared to its increase in power output.

In the case of the foiled blades, we observe a peak C_p of 0.207 with a shroud and 0.286 without a shroud. The increase in C_p without the shroud is accompanied by a 20% increase in peak C_T , which contrasts the trend we observed with the flat blades with and without the shroud (increase in C_p , decrease in C_T). Increases in power are typically accompanied by increases in thrust for axial-flow turbines, so we hypothesize that for the unshrouded, foiled rotor the increase in thrust exceeded the elimination of drag on the shroud in the streamwise direction, producing an overall net increase in thrust.

It is evident that the shroud had a larger impact on efficiency of the foiled blade turbine compared to the flat blade turbine. This is possibly due to specific differences in geometric design; the height of the shroud on the flat and foiled blade turbine were 50 mm and 63 mm, respectively. The larger shroud height on the foiled blade turbine produces more drag opposing the direction of rotation. Furthermore, the flat blades on the shrouded turbine extended from the front edge of the shroud to the back edge of the shroud, while the foiled blades on the shrouded turbine only spanned 71% of the shroud height, which means there was less power production to make up for the increase in drag.

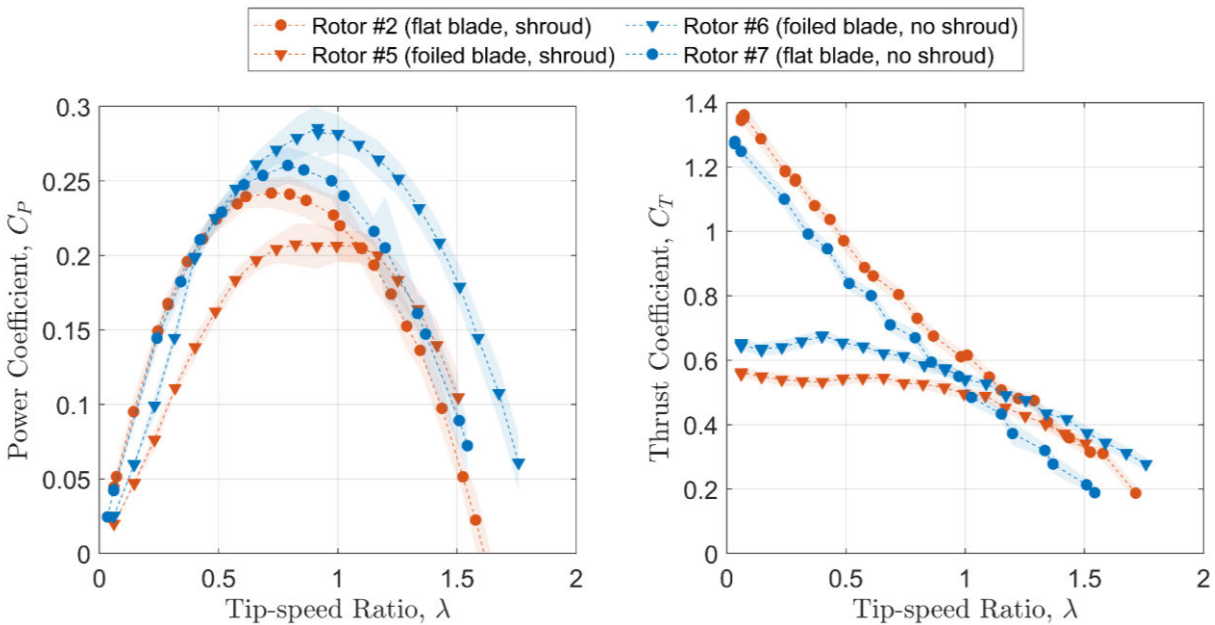


Figure 9. Coefficients of power and thrust as a function of tip-speed ratio for rotors varying in blade type (foiled or flat) and use of shroud. Shaded regions indicate the interquartile range.

Fig. 10 compares four shrouded rotors of varying blade number, 7-11. Each rotor uses flat blades with a height-to-diameter ratio of $\frac{1}{10}$. It is known from previous literature (Burton et al. 2001) that multi-bladed rotors with too many blades will result in each blade interfering with optimal fluid flow across

neighboring blades. With too few blades, there is less blade surface area interacting with the fluid, and the rotor may not effectively capture the available energy in the fluid. In this case, we observe 9 to be the optimal blade number for this rotor design (Fig. 10), which was also found to be true in the CFD simulations preceding this experimental investigation. We note, however, that performance is less sensitive to blade number than to the height-to-diameter ratio, foiled vs. flat profiles, or the inclusion of a shroud.

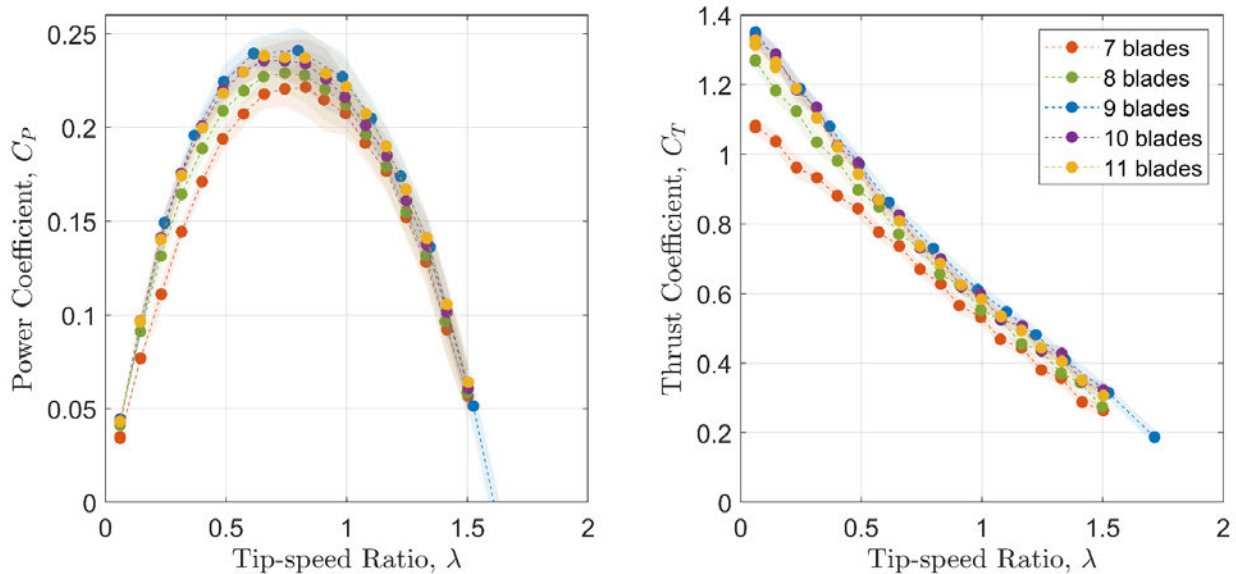


Figure 10. Coefficients of power and thrust as a function of tip-speed ratio for shrouded rotors of varying blade number (7-11). Each rotor uses flat blades with a height-to-diameter ratio of $\frac{1}{3}$. Shaded regions indicate the interquartile range.

7.1.3 Blockage-corrected performance

Flow confinement is known to significantly impact turbine performance. The blockage correction by Barnsley and Wellicome (1990), formally evaluated in Ross and Polagye (2020), was used to estimate the performance of each rotor in unconfined flow based on the confined performance results presented in Figs. 8-10. The blockage corrected data is shown in Figs. 11-13 and is more representative of expected performance at full-scale in open water. General trends observed under confined flow remain the same in the blockage-corrected data, with one notable exception. Between Figs. 8 and 11, we see that in confined flow rotor #2 produces 4.4% more mechanical power than rotor #1, while in unconfined flow, according to the blockage-corrected performances, rotors #1 and #2 both operate at approximately the same peak efficiency (i.e., power coefficient) of 21%. This is because flow confinement effects are a function of both geometric blockage (ratio of swept area to channel cross-sectional area) and rotor thrust. Given the drastic differences in peak thrust between rotors #1 and #2 observed in both the confined and unconfined performance results, further investigation of the performance of these two particular rotors in open water would be helpful in assessing the tradeoffs of each design.

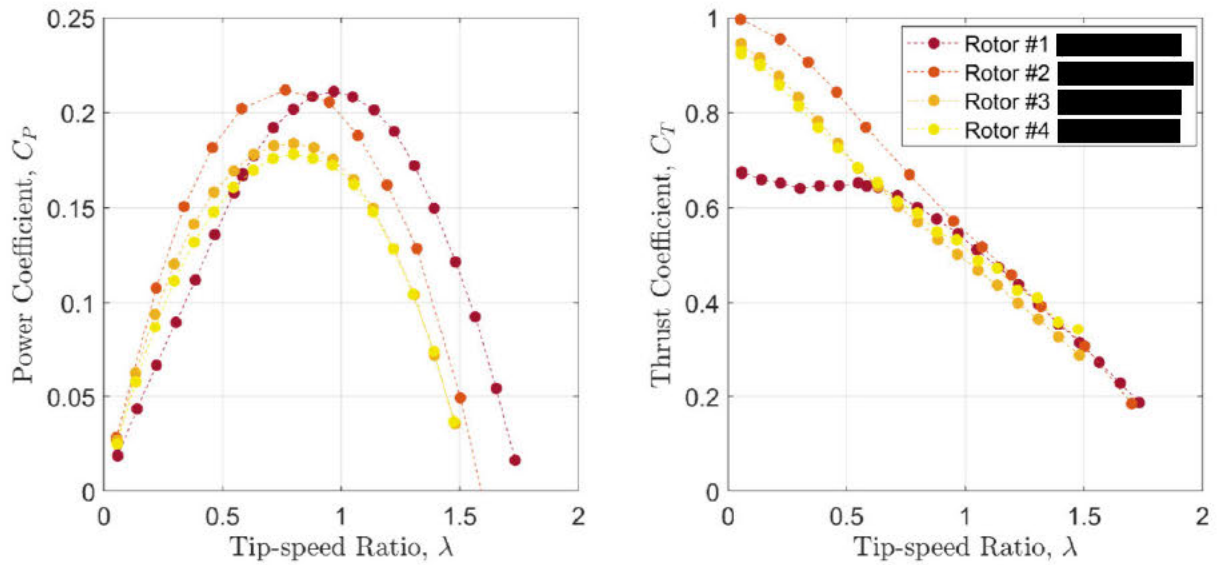


Figure 11. Blockage-corrected coefficients of power and thrust as a function of tip-speed ratio for shrouded rotors of varying height-to-diameter ratios. Shades from dark to light indicate increasing height-to-diameter ratios.

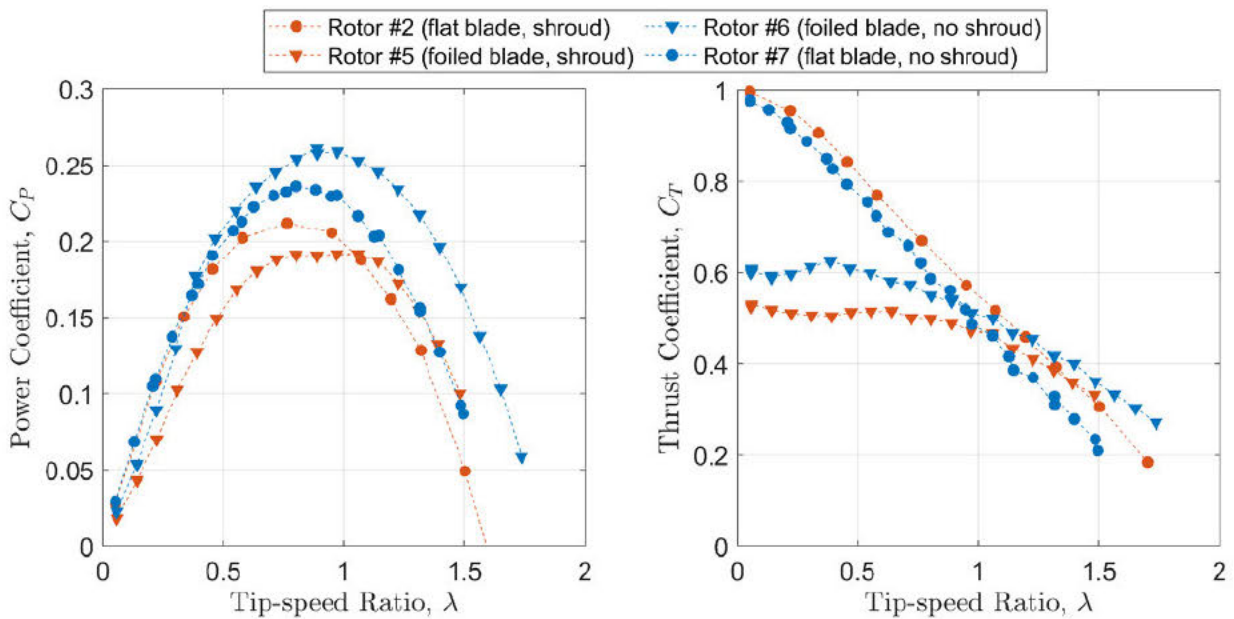


Figure 12. Blockage-corrected coefficients of power and thrust as a function of tip-speed ratio for rotors varying in blade type (foiled or flat) and use of shroud.

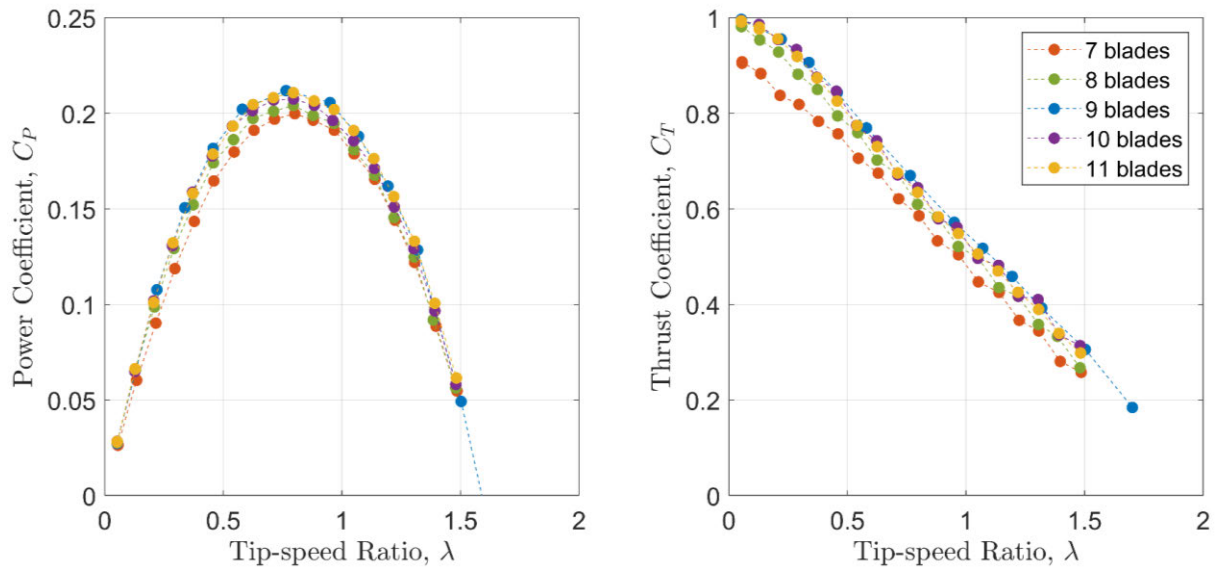


Figure 13. Blockage-corrected coefficients of power and thrust as a function of tip-speed ratio for shrouded rotors of varying blade number (7-11). Each rotor uses flat blades with a height-to-diameter ratio of $\frac{1}{3}$.

7.2 LESSON LEARNED AND TEST PLAN DEVIATION

Two deviations were made from the original test plan: (1) the number of rotors tested, and (2) the use of the encoder on the drive shaft. In the original test plan, we planned to test 5 rotor variants. However, because minimal issues were encountered in commissioning and testing, we were, ultimately, able to test 6 additional rotor variants of interest to Sitkana.

The second deviation followed intermittent issues with the data from the encoder on the drive shaft. Since phase-averaged data was not of interest in this study, we prioritized reliable speed control which was not reliant on the encoder. Stepper motors are known for their precise speed control, and prior testing with this axial-flow turbine has demonstrated that we achieve the commanded rotation rate within 0.3% error. After these experiments concluded, we identified the root cause as the shaft-encoder separation distance moving out of spec when the mounting bolts for the encoder were tightened. This was rectified with additional washers to better distribute pressure from the bolts.

8 CONCLUSIONS AND RECOMMENDATIONS

This research has provided a scale model characterization of the shrouded rotor for Sitkana's hydrokinetic turbine. The goals of this research were to allow Sitkana to (1) refine the optimal rotor geometry, (2) validate their numerical models, and (3) predict power output for a full-scale system. All three of these objectives were met.

The rotor geometry consists of three parameters: height/diameter ratio, twist, and blade number. All three parameters were investigated through computational fluid dynamic modeling, and these results

determined the samples used in flume testing. UW has sent Sitkana data from testing so that Sitkana can compare the results to computational models for validation.

The results are easily convertible to full-scale models, because the tests were all conducted above the Reynold’s independence threshold and were corrected for blockage. Given rotor #1 or rotor #2 with a coefficient of power of 21%, a full-scale rotor diameter of 1 meter, and an operating condition of 2.5 m/s, a full-scale rotor could generate approximately 1.3 kW of mechanical power. This is well-matched with the 1.5kW generators being used in Sitkana’s system.

These results also provide useful information for Sitkana in regard to the net benefit of the various thin-blade rotor designs. An example can be seen in Table 6 comparing several rotors. Rotor #6 did have a higher coefficient of power by about 24% (0.26 compared to 0.21), but when put into a 3D printing slicer program at full-scale, rotor #6 would also use more material due to thicker blades. In addition, rotor #6 also lacks the shroud, which adds structural integrity to the design while potentially reducing wildlife impact and lowering the risk of debris entanglement.

Table 6. Cost-benefit matrix comparing three sample rotors.

Parameter	Rotor #1 (Thin-Bladed, Shrouded)	Rotor #2 (Thin-Bladed, Shrouded)	Rotor #6 (Foiled, Unshrouded)
Peak power coefficient (blockage-corrected)	0.21	0.21	0.26
Peak thrust coefficient (blockage-corrected)	0.68	1	0.63
Thrust coefficient at peak power (blockage-corrected)	0.55	0.67	0.54
Material Usage for a full-scale turbine	6 kg	7 kg	11 kg
Shroud benefits	Yes	Yes	No

Further computational and/or experimental investigations of rotors #1 and #2 in unconfined flow are recommended, based on the similarity in peak power coefficients between the two rotors in the blockage-corrected performance results. Rotor #1 offers reduced peak thrust loads, as well as reduced thrust at the optimal tip-speed ratio, and lower material costs relative to rotor #2. However, the accuracy of blockage corrections can vary, so further study of these two particular rotors in open water would be helpful in assessing the tradeoffs of each design. Due to the visible deflection seen in blades without a shroud, it would also be useful to identify the necessary blade thickness for survivability, which would affect the material usage of each design, and assess whether the increased performance (if consistent at greater blade thicknesses) outweighs the increased material cost and potential environmental impacts.

9 REFERENCES

T Burton, D Sharpe, N Jenkins, E Bossanyi, 2001. Wind Energy Handbook. West Sussex, England: John Wiley & Sons Ltd.

MG Borg, Q Xiao, S Allsop, A Incecik, C Peyrard, 2020. A numerical performance analysis of a ducted, high-solidity tidal turbine. *Renewable Energy*, 159, pp. 663-682.

MJ Barnsley and JF Wellicome, 1990. Final report on the 2nd phase of development and testing of a horizontal axis wind turbine test rig for the investigation of stall regulation aerodynamics. Technical Report E.5A/CON5103/1746, ETSU.

H Ross and B Polagye, 2020. An experimental assessment of analytical blockage corrections for turbines. *Renewable Energy*, 152, pp. 1328-1341.

H Ross and B Polagye, 2022. Effects of dimensionless parameters on the performance of a cross-flow current turbine. *Journal of Fluids and Structures*, 114.

K Van Ness, C Hill, J Burnett, A Aliseda, B Polagye, 2021. Experimental comparison of blade pitch and speed control strategies for horizontal-axis current turbines. *Journal of Ocean Engineering and Marine Energy*, 7(1), pp. 83-96.

10 ACKNOWLEDGEMENTS

The UW would like to thank the Alice C. Tyler Charitable Trust for their support of experimental facilities, including the Alice C. Tyler Flume.

11 APPENDICES

11.1 APPENDIX A: REYNOLDS-INDEPENDENCE

After verifying Reynolds-independence with rotor #2, the remaining rotors were tested in both 0.55 m/s and 0.77 m/s flow to confirm Reynolds-independence for the new geometry. Figs. 14-23 demonstrate that the remaining rotors were also tested in a Reynolds-independence regime. The subtle changes near the peak in the power coefficient, though within our experimental uncertainty, may be due to a difference in the submergence-based Froude number based on a similar trend seen in Ross and Polagye (2022) for changes in submergence-based Froude number. Our free surface transducer measurements from the 0.55 and 0.77 m/s cases reveal a 1-cm difference in dynamic depth between the two flow conditions, which corresponds to a change in blockage from 15.5% to 15.8% and a change in submergence-based Froude number from 0.45 to 0.66. Any potential impact on performance due to these differences was observed to be less than our experimental uncertainty, so no adjustments were made to the fill height between experiments, which would have severely limited the number of tests we could perform due to the time required to reach thermal equilibrium.

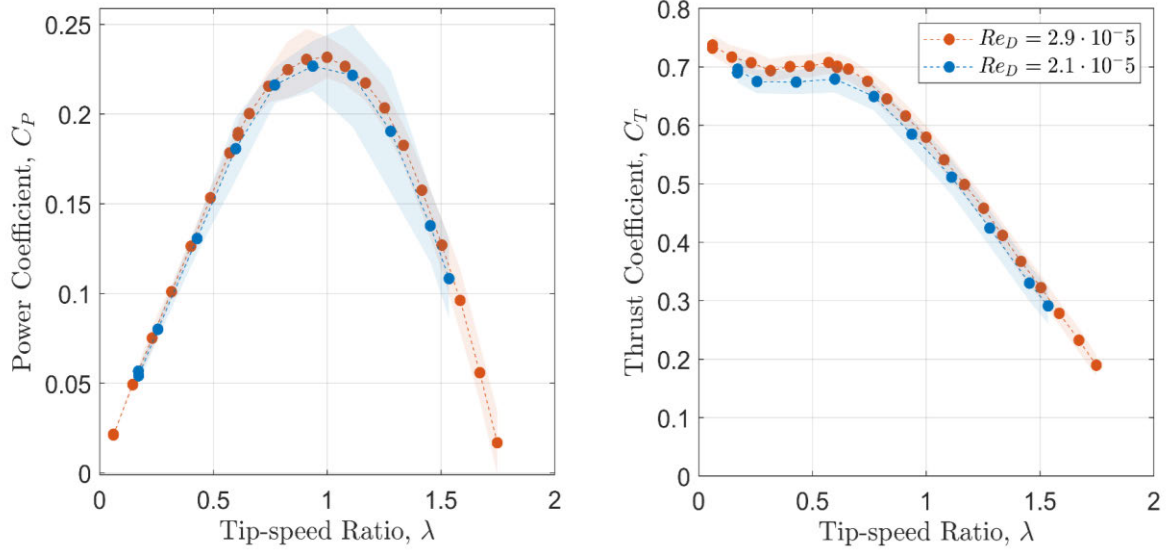


Figure 14. Coefficients of power and thrust as a function of tip-speed ratio for rotor #1 in 0.55 and 0.77 m/s inflow. Shaded regions indicate the interquartile range.

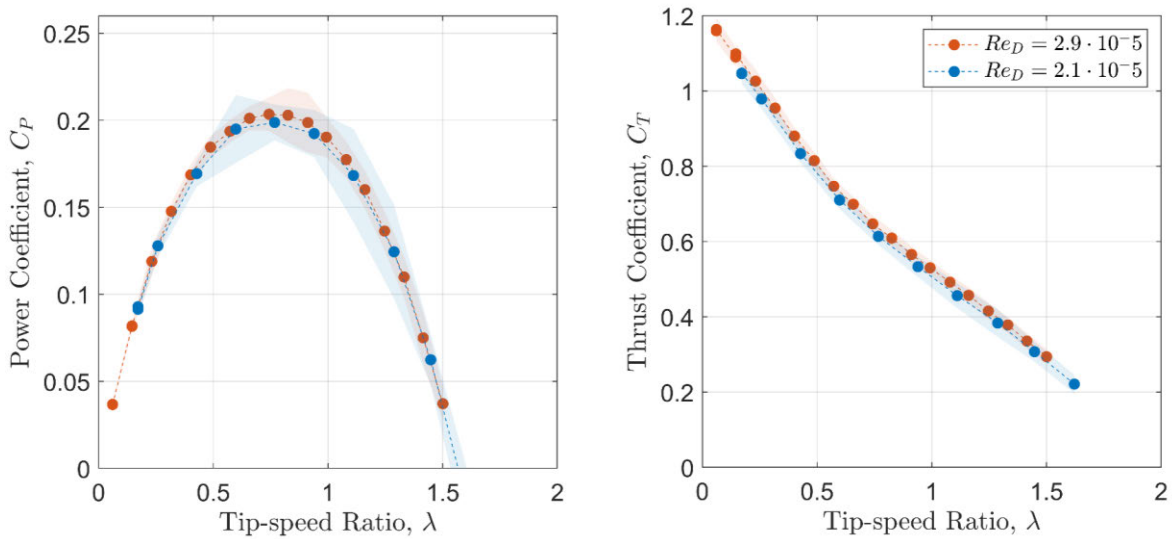


Figure 15. Coefficients of power and thrust as a function of tip-speed ratio for rotor #3 in 0.55 and 0.77 m/s inflow. Shaded regions indicate the interquartile range.

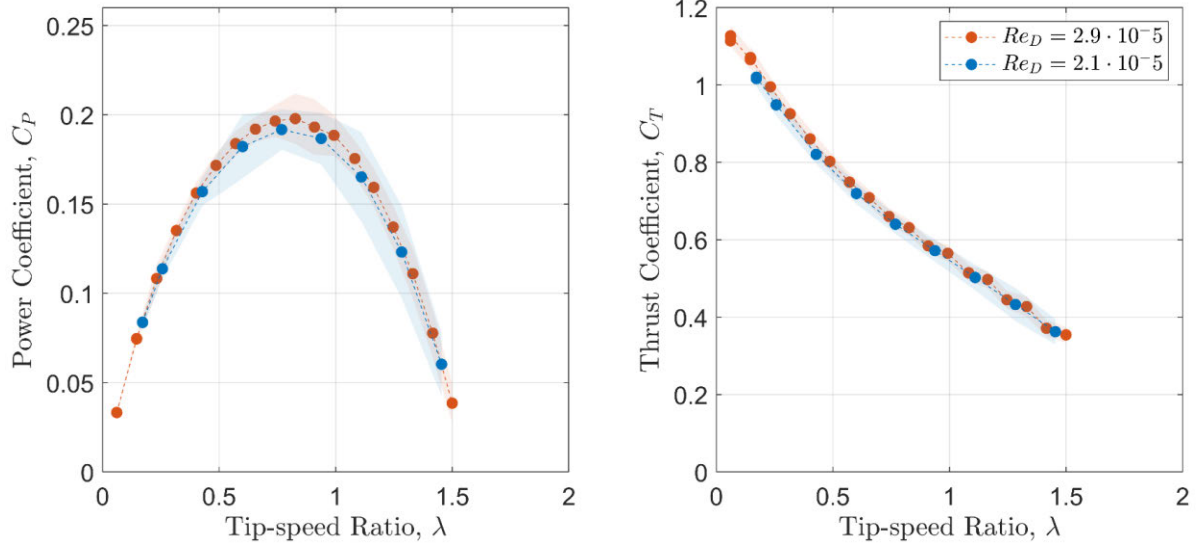


Figure 16. Coefficients of power and thrust as a function of tip-speed ratio for rotor #4 in 0.55 and 0.77 m/s inflow. Shaded regions indicate the interquartile range.

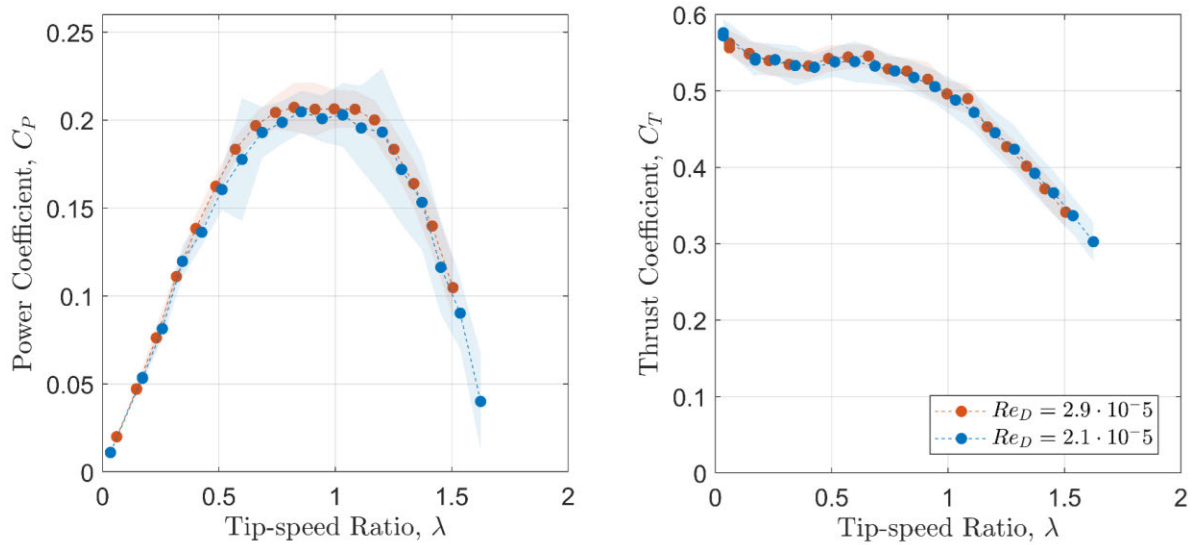


Figure 17. Coefficients of power and thrust as a function of tip-speed ratio for rotor #5 in 0.55 and 0.77 m/s inflow. Shaded regions indicate the interquartile range.

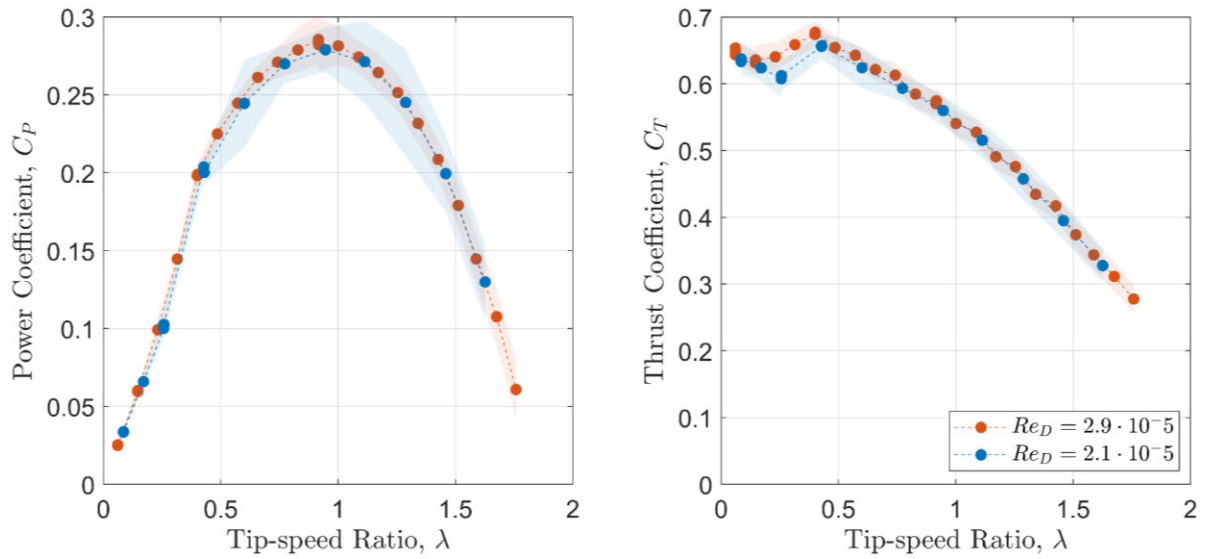


Figure 18. Coefficients of power and thrust as a function of tip-speed ratio for rotor #6 in 0.55 and 0.77 m/s inflow. Shaded regions indicate the interquartile range.

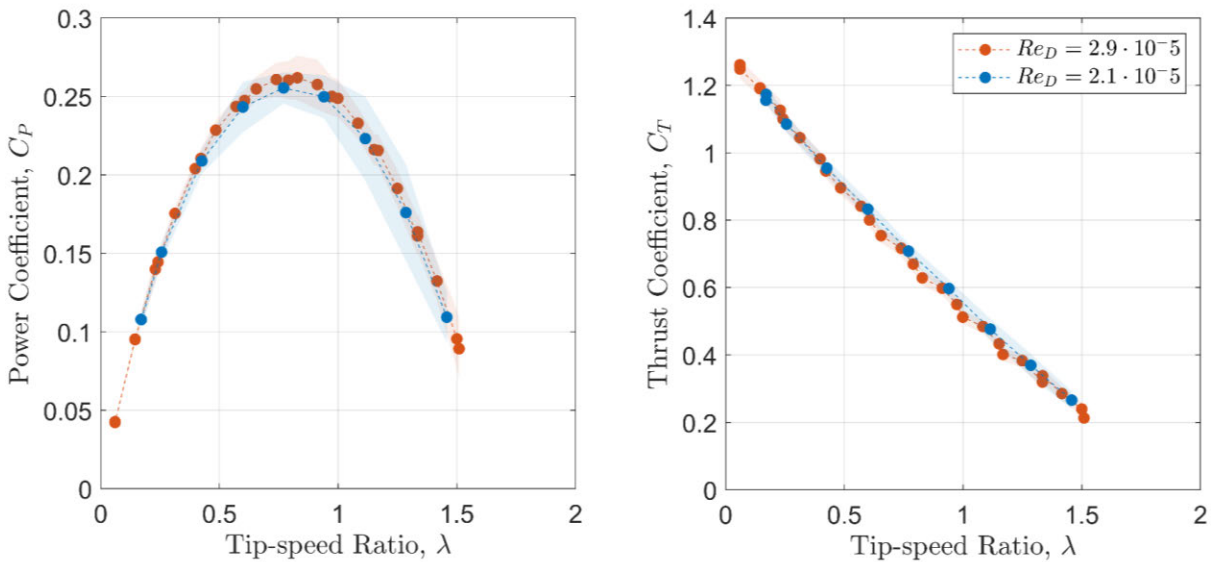


Figure 19. Coefficients of power and thrust as a function of tip-speed ratio for rotor #7 in 0.55 and 0.77 m/s inflow. Shaded regions indicate the interquartile range.

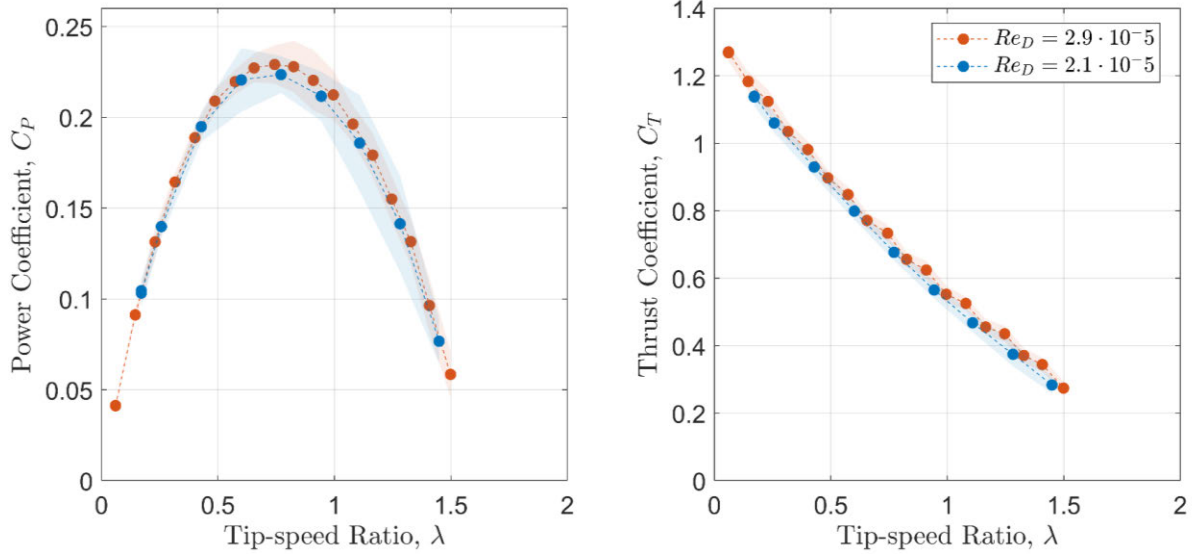


Figure 20. Coefficients of power and thrust as a function of tip-speed ratio for rotor #8 in 0.55 and 0.77 m/s inflow. Shaded regions indicate the interquartile range.

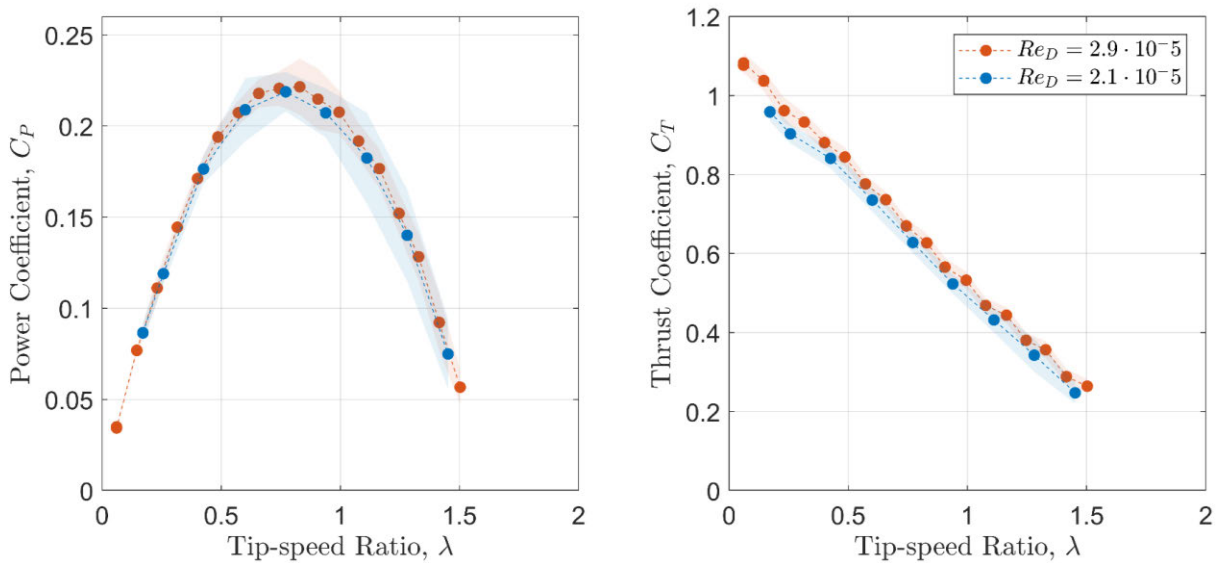


Figure 21. Coefficients of power and thrust as a function of tip-speed ratio for rotor #9 in 0.55 and 0.77 m/s inflow. Shaded regions indicate the interquartile range.

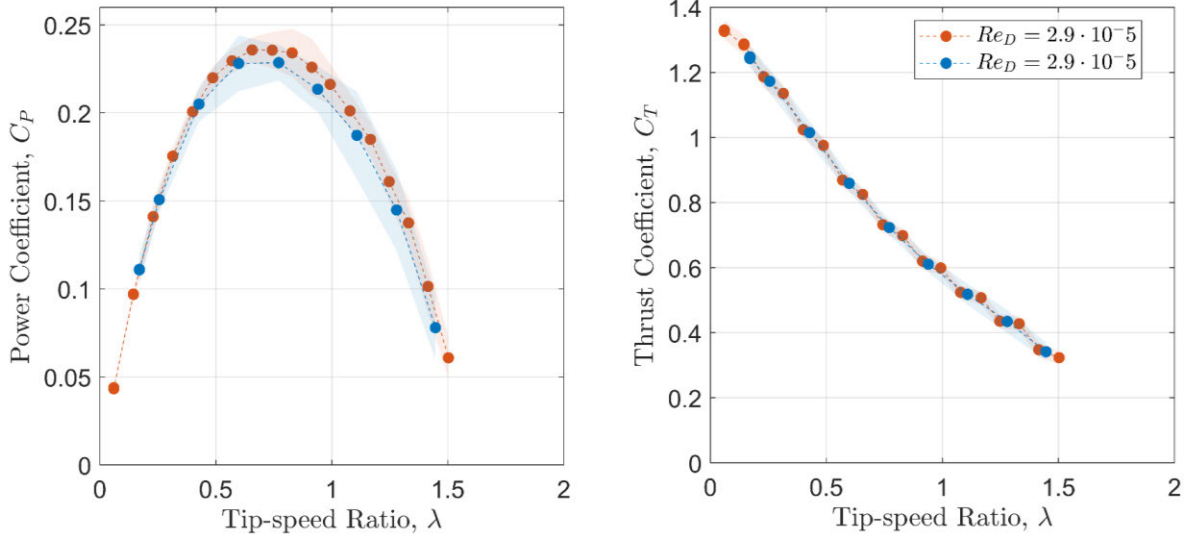


Figure 22. Coefficients of power and thrust as a function of tip-speed ratio for rotor #10 in 0.55 and 0.77 m/s inflow. Shaded regions indicate the interquartile range.

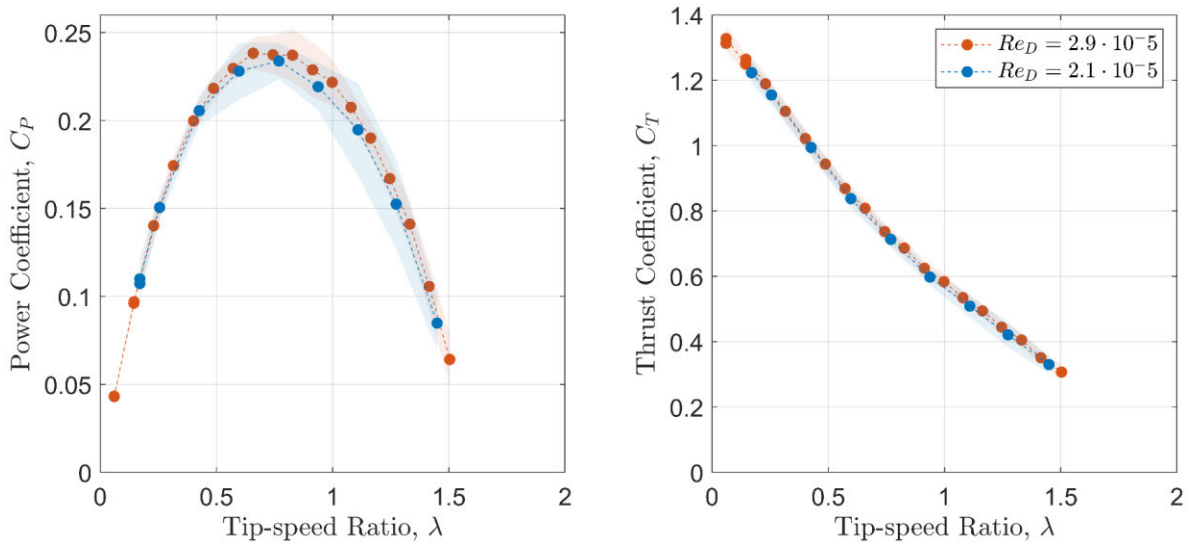


Figure 23. Coefficients of power and thrust as a function of tip-speed ratio for rotor #11 in 0.55 and 0.77 m/s inflow. Shaded regions indicate the interquartile range.

11.2 APPENDIX B: REPEATABILITY

Rotor #2 was repeatedly tested throughout the campaign to confirm repeatability across testing days. In Fig. 24, we observe across all 5 tests over a 3 week period, the power coefficient was consistently measured within a 0.01 spread and the thrust coefficient was consistently measured within a 0.06 spread.

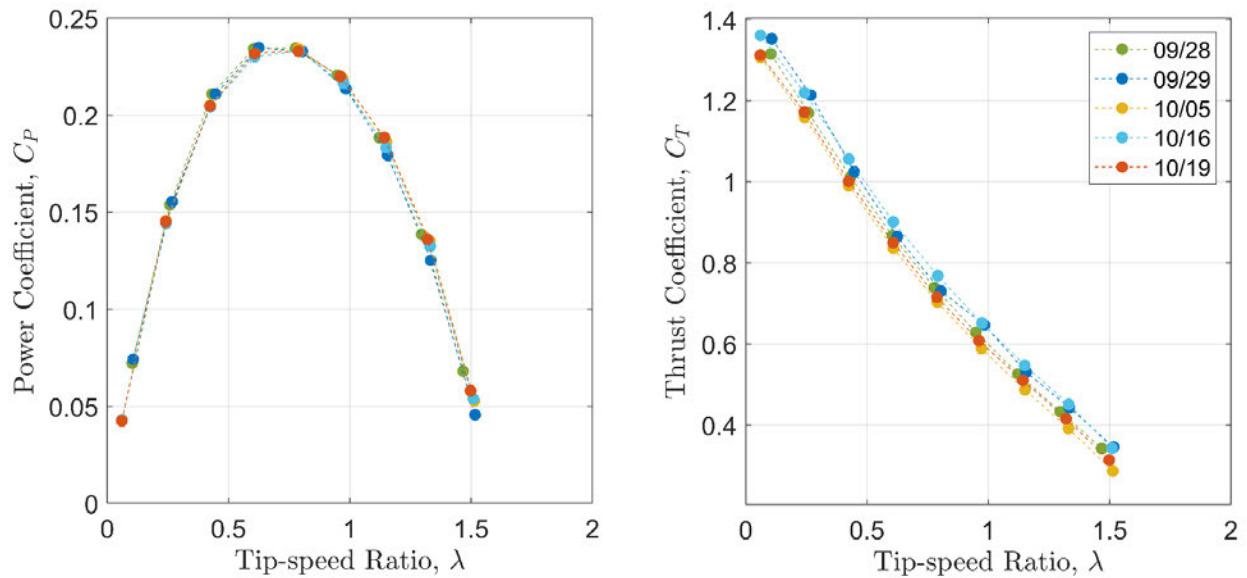


Figure 24. Coefficients of power and thrust as a function of tip-speed ratio for rotor #2 (flat blades, shrouded, height-to-diameter ratio of ██████) used as a baseline to check for consistency and repeatability across the testing period.